Enhancing the hydrodesulfurization of 4,6-dimethyldibenzothiophene through the use of mixed mows2 phase evidenced by haadf

M. S. Nikul'Shina, A. V. Mozhaev, Christine Lancelot, Pascal Blanchard, Maya Marinova, Carole Lamonier, P. A. Nikul'Shin

Enhancing the hydrodesulfurization of 4,6-dimethyldibenzothiophene through the use of mixed $MoWS_2$ phase evidenced by HAADF

M. Nikulshina[a,b], A. Mozhaev[a], C. Lancelot[b], P. Blanchard[b], M. Marinova[c], C. Lamonier[b*], P. Nikulshin[a,d*]

[a] Samara State Technical University, 244 Molodogvardiyskaya St., Samara 443100, Russia

[b] Université Lille1, UMR 8181 CNRS, UCCS, Villeneuve d'Ascq, France

[c] Institut Chevreul, University of Lille & CNRS, Villeneuve dAscq F-59655, France

[d] All-Russia Research Institute of Oil Refining, 6/1 Aviamotornaya st., Moscow 111116, Russia

[*]Corresponding author. Tel/Fax: +7 846 2423580

E-mail: p.a.nikulshin@gmail.com (Pavel Nikulshin), carole.lamonier@univ-lille1.fr (Carole Lamonier)

Abstract

MoW alumina supported hydrotreating (HDT) catalysts were synthesized by using mixed $SiMo_nW_{12-n}$ heteropolyacids (HPAs) and from a mixture of $SiMo_{12}$ and SiW_{12} HPAs with the same Mo/W ratios for reference. Gas phase sulfidation of the catalysts prepared from mixed MoW HPAs led to the formation of a mixed phase evidenced by high-angle annular dark-field (HAADF) images, where a core of Mo atoms was surrounded by W atoms. Contrariwise mostly MoS_2 or WS_2 slabs were observed in the solids prepared from a mixture of the HPAs. This mixed phase induced higher hydrodesulfurization (HDS) of DBT as well as hydrogenation (HYD) of naphthalene than in the case of the reference catalysts. Comparison of activation procedures (gas phase versus liquid phase) confirmed that sulfidation in gas phase led to more efficient catalysts, even in the case of the formation of the mixed slabs. Beneficial effect of the mixed MoWS phase was even more pronounced in the case of the HDS of a more refractory molecule, 4,6-

dimethyldibenzothiophene (4,6-DMDBT), which was attributed to the more hydrogenating properties of this mixed phase.

Keywords: Hydrodesulfurization; Hydrogenation; Heteropolyanion; MoW catalysts; DBT; 4,6-DMDBT.

1. Introduction

A release of new stringent standards on the sulfur concentration in the transportation fuels led to an intense research activity on HDS. Conventional Co(Ni)-promoted Mo(W) alumina supported HDT catalysts exhibit high activity in removing sulfur from thiophene and dibenzothiophene (DBT) compounds. However, deep desulfurization and production of ultra-low sulfur fuels are compounded by the presence of resistant molecules such as alkyl-substituted DBTs. Alkyl groups in the 4 and 6 positions in DBT molecules make them more resistant to HDS due to the steric hindrance around the sulfur atom [1]. The HDS of 4,6-DMDBT goes through two reaction pathways: direct desulfurization (DDS) via σ-bonding of the molecule to the catalyst surface with breaking of the C–S bonds and hydrogenation (HYD) via π-bonding with preliminary hydrogenation of one aromatic ring, giving preference to the latter [2,3]. Considering this fact the development of a new generation of catalysts with high HYD activity is a topical task.

Subsequent to the development of high-active bulk NiMoW HDS catalyst (NEBULA) [4] many studies were devoted to investigation of this system. Supported MoW catalysts were also investigated and were prepared from a mixture of conventional ammonium heptamolybdate and ammonium metatungstate or of tetrathiomolybdate and tetrathiotungstate leading to better thiophene HDS catalytic performances [5,6]. Despite these trimetallic NiMoW sulfide catalysts have a potential advantage over bimetallic Ni-Mo and Ni-W systems, in respect to deep sulfur [7-10], precise determination of the reasons of high activity of these catalysts is not simple.

Nowadays the use of heteropolycompounds as starting oxidic precursor of an active phase is an interesting alternative method for preparation of HDS catalysts with improved catalytic

properties [11-19]. In the field of hydrotreatment catalysis, Keggin and Keggin-derivated heteropolymolybdate and heteropolytungstate structures have been successfully used to replace conventional precursors. Thus, Ni promoted molybdenum and tungsten HPA-based catalysts showed better performance in deep HDS of 4,6-DMDBT [20] and diesel hydrotreating [21] than the counterparts prepared from traditionally used Mo (W) ammonium salts.

We proposed recently a new approach to prepare (Ni)MoW catalysts using mixed MoW HPA, allowing to introduce together Mo and W from a single molecular entity [22]. Mo_nW_{12-n}/Al_2O_3 mixed HPAs based catalysts sulfided with dimethyl disulfide (DMDS) in liquid phase were found more efficient in the HDS of DBT and HYD of naphthalene than their counterparts obtained by a mixture of monometallic HPAs with the same Mo/W ratio. Moreover, these catalysts had improved HYD properties, which was related to the formation of a mixed Mo-W sulfide phase after liquid phase sulfidation. The procedure of activation of oxide precursors to the active sulfide phase plays an important role and influences to the structure and properties of active phase particles [23-26]. In addition, Hensen and co-workers [27] have recently shown that sulfidation conditions of trimetallic $NiMoW/Al_2O_3$ catalysts prepared from separate Mo and W precursors led to different morphology of active phases and to different catalytic properties. The most commonly used procedures consist in gas phase sulfidation (GS) under a flowing H_2S/H_2 while liquid phase sulfidation (LS) is performed through the use of sulfiding agents (CS_2, dimethyl sulfide, DMDS and etc.).

In the present study, mixed HPA based catalysts are activated under gas phase and characterized by XPS, HRTEM and HAADF. Their catalytic performances are evaluated in the HDS of DBT and also in a more refractory molecule, 4,6-DMDBT, as well as in naphthalene HYD. A particular attention is also paid to the comparison of sulfidation methods (gas versus liquid phase) and its effect on the nature of the active phase and location of Mo and W atoms in sulfide slabs thanks to the use of HAADF.

2. Experimental

2.1 Catalyst preparation

Hydrotreating catalysts with the same surface density of metals d(Mo+W) ≈ 4 at/nm^2 were synthesized by the incipient wetness method via impregnation of Al_2O_3 extrudates (S_{BET} = 235 m^2/g, V_p = 0.9 cm^3/g) with aqueous solutions containing the required amounts of HPAs [22]. Two bimetallic Mo_1W_{11}/Al_2O_3 and Mo_3W_9/Al_2O_3 catalysts were prepared by using corresponding mixed $SiMo_1W_{11}$ and $SiMo_3W_9$ HPAs. Two $(Mo_n+W_{12-n})/Al_2O_3$ reference catalysts were also prepared using mixture of monometallic $SiMo_{12}$ and SiW_{12} HPAs with a same Mo/W ratio as in mixed ones. Finally, Mo_{12}/Al_2O_3 and W_{12}/Al_2O_3 samples based on corresponding monometallic HPAs were synthesized for comparison. The oxidic catalyst precursors after maturation were dried at 100 ºC for 10 h in air atmosphere without further calcination. The chemical compositions of the prepared catalysts are given in Table 1.

Prior the characterization of the active phase of the catalysts and evaluation of their catalytic activities, the solids were activated by gas phase sulfidation, which was carried out in one step under a flow of a mixture of 10 % of H_2S into H_2 at atmospheric pressure with heating to 400 ºC over a holding period of 2 h.

2.2 Catalyst characterization

2.2.1 High-resolution transmission electron microscopy (HRTEM)

HRTEM characterization of sulfided $Mo(W)/Al_2O_3$ catalysts was performed using a Tecnai G2 20 electron microscope with a 0.14 nm lattice-fringe resolution and an accelerating voltage of 200 kV. Slab length and layer stacking distributions of $Mo(W)S_2$ crystallites in each catalyst were estimated on the observations of at least 500 crystallites taken from different parts of the same sample. The average length of the slab ($\bar{L}$) was calculated as simple arithmetic mean and approximately corresponds to the diagonal dimension of the observed $Mo(W)S_2$ slab [28]. The number of slabs per stack was determined to obtain the average stacking degree ($\overline{N}$):

$$\overline{N} = \frac{\sum_{i=1..t} n_i N_i}{\sum_{i=1..t} n_i}, \quad (1)$$

where n_i is the number of stacks in N_i layers.

2.2.2 High resolution high-angle annular dark-field scanning transmission electron microscopy (HR HAADF-STEM)

HAADF-STEM analyses were performed using a FEG TEM/STEM system (Titan Themis FEI) operated at 200 kV, equipped with a monochromator and a probe Cs corrector. For HAADF acquisition, the spot size was 9 with a screen current of ~50 pA and a camera length of 115 mm, corresponding to inner and outer diameters of annular detector of ~50 and ~200 mrad, respectively. Freshly sulfided samples were ground under an inert atmosphere and dispersed in ethanol. The suspension was collected on carbon films supported on copper grids.

2.2.3 X-ray photoelectron spectroscopy (XPS)

The sulfided catalyst samples were analysed by XPS. The spectra were obtained on a Kratos Axis Ultra DLD spectrometer using a monochromatic AlK_α source (hν = 1486.6 eV, 150 W). The binding energy (BE) scale of the spectrometer was preliminarily calibrated using the position of the peaks for the Au $4f_{7/2}$ (83.96 eV) and Cu $2p_{3/2}$ (932.62 eV) core levels of pure metallic gold and copper. The samples were mounted on a holder using double-sided adhesive tape. The analysis chamber was operated under ultrahigh vacuum with a pressure close 10^{-10} Torr. For the non-conductive samples, the Kratos charge neutraliser system was used, and the spectra were charge-corrected to provide the Al 2p spectral component at 74.6 eV. In addition to the survey photoelectron spectra, narrow spectral regions (Al 2p, S 2p, Mo 3d, W 4f, C 1s and O 1s) were recorded. The pass energy of the analyser was 160 eV for the survey spectra and 40 eV for the narrow scans. The individual spectral regions were analysed to determine the BE of the peaks, identify the chemical state of the elements and calculate the relative ratios of the elements on the

catalyst surface. The collected spectra were analysed using the CasaXPS software program (Version 2.3.16) after applying a Shirley background subtraction. Gaussian (30 %) – Lorentzian (70 %) peaks were used for spectra decomposition.

XPS decomposition enabled the absolute quantification of each species:

$$C(i)_{\mathrm{T}}\ (\text{at. \%}) = \frac{A_i / S_i}{\sum_{i=1..n} A_i / S_i} \times 100, \qquad (2)$$

where A_i is the measured area of species i, S_i is the sensitivity factor of the atom related to species i (based on Wagner cross sections and on transmission factors provided by the manufacturer) and $C(i)_{\mathrm{T}}$ is the absolute content of species j.

Fig. 1 shows the examples of spectra of Mo 3d, W 4f and S 2p photoelectron spectra recorded for Mo_3W_9/Al_2O_3 catalyst. It is well known that after sulfidation of Mo or W based catalysts three main W and three main Mo contributions can be identified:

- for W particles: a W^{4+} species of the WS_2 phase characterized by a doublet ($W4f_{7/2}$ and $W4f_{5/2}$) with a BE at about 32.1 and 34.3 eV, , a W^{5+} species of W^{V}-OS oxysulfide species at about 33 and 35.2 eV and a doublet at 36 and 37.9 eV correlated with W^{6+} oxide species (W^{VI}-O).

- for Mo particles: a doublet at about 229 eV and 232 eV ($Mo3d_{5/2}$ and $Mo3d_{3/2}$) correspond to the MoS_2 species. A doublet at about 230 and 233.5 eV is related to oxysulfide species (Mo^{V}-OS) and a doublet at about 232.5 and 235.7 eV is correlated with Mo^{6+} oxide species (Mo^{VI}-O).

S2p spectra are known to evidence two contributions assigned to sulfide (226 eV) and oxysulfide entities (227.5 eV).

Contact with air (oxygen) was clearly avoided after activation during the transfer in the XPS chamber preventing oxygen contamination, sulfate species are in this case formed during the activation procedure. The absence of any signal at 169.0 eV in the S2p XPS spectra (characteristic of sulfates) indicates that sulfided catalysts were not reoxidized during the transfer of the solid from the sulfiding reactor to the XPS instrument.

To obtain more information about the nature of the Mo and W species, all the XPS spectra were carefully decomposed thanks to previous works [29-33] but also using the appropriate oxide and sulfided references as supported monometallic catalysts for examples. Indeed, several steps are necessary to obtain meticulous decompositions.

2.2.3.1 Decomposition of Mo 3d spectra

In sulfided molybdenum catalysts, Mo and S coexist. The spectral envelope of Mo3d covers the energy range of 227–238 eV as the chemical oxidation states of Mo vary from 0 to +VI, while that of S2s covers the 224–235 eV range, which corresponds to S chemical states varying from -II to +VI leading to the overlapping of both Mo3d and S2s BE regions. The contribution of S2s must be thus initially ruled out to obtain the true one of Mo3d level. The BE, full width at half maximum (FWHM) and a peak area of S2s contributions were directly deduced from those of the corresponding S2p peaks using the constraints reported in Table 2. Each S2p contribution was thus simulated with two interdependent peaks corresponding to $S2p_{1/2}$ and $S2p_{3/2}$ core levels taking into account the constraints in the area, FWHM and position as reported in Table 2. For example, all the constraints concerning S2p and S2s levels were refined thanks to the XPS analysis of the sulfided W_{12}/Al_2O_3 catalyst.

Each Mo contribution was simulated with a doublet corresponding to $Mo3d_{3/2}$ and $Mo3d_{5/2}$ core levels. The spectral characteristics of $Mo3d_{3/2}$ and $Mo3d_{5/2}$ peaks being interdependent, each doublet was simulated using constraints in the area, FWHM and BE as well reported in Table 2 (these constraints being deduced from theoretical considerations and/or refined from experimental data).

The values of areas, FWHM and positions of BE of the main $S2p_{3/2}$, S2s and $Mo3d_{5/2}$ XPS peaks (A, B, C, D, E, F, G) were calculated by the CASA software to obtain good correlation between the experimental XPS spectra and the corresponding simulated ones while respecting all the constraints which were imposed between these peaks and all other peaks.

2.2.3.2 Decomposition of W 4f spectra

The decomposition of W4f spectra must be undertaken cautiously, especially when the analyzed solids contain molybdenum. Indeed the $W5p_{3/2}$ and Mo4p (non splitted level) BE ranges overlap that of W4f level. Therefore, the contributions of these peaks must be also ruled out to obtain the true one of W4f level. The BE, FWHM and areas of Mo4p contributions were directly deduced from those of the corresponding $Mo3d_{3/2}$ peaks using the constraints reported in Table 3 since their spectral characteristics can be considered as being interdependent. All the constraints linking BE, FWHM and areas of Mo4p and $Mo3d_{3/2}$ peaks were experimentally deduced thanks to the XPS analysis of the oxidic Mo_{12}/Al_2O_3 catalyst.

The spectral characteristics of $W5p_{3/2}$, $W4f_{5/2}$ and $W4f_{7/2}$ are also interdependent. So the W4f contributions were simulated with doublets corresponding to $W4f_{5/2}$ and $W4f_{7/2}$ core levels. Each doublet was simulated using constraints in the area, FWHM and BE as well reported in Table 3. $W5p_{3/2}$ was simulated with one peak with BE, FWHM and area linked to the $W4f_{7/2}$ corresponding one (Table 3). All the constraints linking $W5p_{3/2}$, $W4f_{5/2}$ and $W4f_{7/2}$ were deduced from experimental data obtained after analysis of oxidic W_{12}/Al_2O_3 catalyst.

The values of areas, FWHM and BE of the main $W4f_{7/2}$ XPS peaks (H, I, J) were calculated by the CASA software to obtain good correlation between the experimental XPS spectra and the corresponding simulated ones while respecting all the constraints which were imposed between these peaks and all other peaks.

The relative concentrations of each species Mo^{VI}-O, Mo^{V}-OS, MoS_2, W^{VI}-O, W^{V}-OS and WS_2 were determined for every sulfided catalyst and were reported in Table 4. For example, the relative amount of WS_2 was determined using the following equation:

$$[WS_2]\,(\%) = \frac{A_{WS_2}}{A_{WS_2} + A_{W^{V}\text{-OS}} + A_{W^{VI}\text{-O}}} \times 100, \qquad (3)$$

where A_X represents the peak area of species x.

2.3 Examination of the catalytic activities

Catalytic properties of synthesized catalysts were investigated in co-hydrotreating of model feed containing DBT (Aldrich, 1500 ppm of S), 4,6-DMDBT (Aldrich, 300 ppm of S) and naphthalene (Aldrich, 3 wt.%) in toluene as a solvent (separate experiments showed that toluene did not undergo hydrogenation under chosen reaction conditions). Prior to testing, the catalysts were activated by the method described above in Section 2.1. The HDT activity tests were performed in a fixed-bed microreactor at 320 ºC, 3.0 MPa of hydrogen, with a LHSV (liquid hourly space velocity) of 10 h^{-1} and a 500 NL/L volume ratio of hydrogen to feed. In a typical HDT reaction, 0.6 g sample of the catalyst (0.25 – 0.50 mm) was diluted with 0.6 cm^3 of low-surface-area carborundum (0.2 – 0.4 mm) and placed in the center of the reactor (the reactor had an internal diameter of 0.8 cm). The liquid product compositions of the samples collected every 1.0 h were determined using a Crystall-5000 Gas Chromatograph equipped with a 30 m OV-101 column. The reaction products were identified by matching retention times with those of commercially available standards and by GC/MS analysis using a Finnigan Trace DSQ. All catalysts exhibited stable performance, achieving a steady state after 7 – 10 h on stream.

The rate constants of the pseudo-first-order reactions of the DBT (4,6-DMDBT) HDS and naphthalene HYD were determined using the following equations:

$$k_{HDS}^{DBT} = -\frac{F_{\mathrm{DBT}}}{W}\ln(1-x_{\mathrm{DBT}}),\ k_{HDS}^{4,6-DMDBT} = -\frac{F_{4,6-DMDBT}}{W}\ln(1-x_{4,6-DMDBT})$$

$$\text{and } k_{\mathrm{HYD}} = -\frac{F_{\mathrm{Naph}}}{W}\ln(1-x_{\mathrm{Naph}}), \tag{4}$$

where k_{HDS}^{DBT}, $k_{HDS}^{4.6-DMDBT}$ and k_{HYD} are the pseudo-first-order reaction constants for the DBT, 4,6-DMDBT HDS, and naphthalene HYD (mol g^{-1} h^{-1}), respectively, x_{DBT}, $x_{4.6-DMDBT}$ and x_{Naph} are the conversions (%) of DBT, 4,6-DMDBT and naphthalene, respectively, F_{DBT}, $F_{\text{4.6-DMDBT}}$ and F_{Naph} are the reactant flow in moles (mol h^{-1}) and W is the weight of the catalyst (g).

The HDS products from DBT included biphenyl (BP) via the direct desulfurization (DDS) pathway, as well as cyclohexylbenzene (CHB) and dicyclohexyl (DCH) from the HYD pathway. Only traces of hydrogenated tetrahydro- and perhydrodibenzothiophenes were observed. The HYD/DDS selectivity was calculated according to the reaction network for DBT HDS (**Scheme 1**):

$$S_{HYD/DDS} = \frac{k_{\mathrm{HYD}}}{k_{\mathrm{DDS}}} = \frac{C_{\mathrm{CHB}} + C_{\mathrm{DCH}}}{C_{\mathrm{BP}}}, \quad (5)$$

where C_{CHB}, C_{BCH} and C_{BP} are the concentrations (mol. %) of CHB, DCH and BP in the reaction products, respectively.

The products of the HDS of 4,6-DMDBT were 3,3′-dimethylbiphenyl (3,3′-DMBP) from DDS pathway and were 1-methyl-3-(2-methylphenyl) cyclohexane (which we will refer to as methylcyclohexyltoluene (MCHT)) and 3,3′-dimethylbicyclohexyl (3,3′-DMBCH) from a hydrogenation pathway (HYD). Only traces of hydrogenated species 4,6-tetrahydro- and perhydrodibenzothiophenes were observed. The HYD/DDS selectivity was calculated according to the reaction network for DBT HDS (**Scheme 2**):

$$S_{HYD/DDS} = \frac{k_{\mathrm{HYD}}}{k_{\mathrm{DDS}}} = \frac{C_{\mathrm{MCHT}} + C_{3,3'\text{-DMBCH}}}{C_{3,3'\text{-DMBP}}}, \quad (6)$$

where C_{MCHT}, $C_{3,3'\text{-DMBCH}}$ and $C_{3,3'\text{-DMBP}}$ are the concentrations (mol. %) of MCHT, 3,3′-DMBCH and 3,3′-DMBP in the reaction products, respectively.

3. Results and discussion

3.1 Characterization of Mo(W)/Al_2O_3 catalysts after activation under H_2/H_2S and their performance in co-HDT of DBT and naphthalene

3.1.1 Sulfidation degree of Mo and W after activation under H_2/H_2S.

The sulfidation degree of Mo and W in all samples was evaluated by XPS after gas phase activation (Table 4). The sulfidation degree of molybdenum was higher than 80 rel. % in all Mo containing samples and varied less than 10 %. Both catalysts prepared from a mixture of two HPAs

had slightly higher sulfidation degree of Mo compared to mixed HPAs based ones. The W sulfidation degree was lower than those obtained for Mo, between 51 and 77%, in agreement with data reported in [22,27,30]. Incorporation of one molybdenum atoms into the structure of HPA had no significant effect on W sulfidation while replacing of three W atoms to Mo ones led to an increase of W content in WS_2 phase compared to W/Al_2O_3 catalyst from 51 to 64 rel. %. Raise of tungsten sulfidation degree with increasing of molybdenum content was also observed for both MoW reference catalysts.

3.1.2 Morphology of the active Mo(W)S_2 phase after activation under H_2/H_2S

Typical HRTEM micrographs of gas sulfided $Mo(W)/Al_2O_3$ are presented in Fig. 2. The black, thread-like fringes are the $Mo(W)S_2$ crystallites with 0.65 nm interplanar distances. The average dimension of the $Mo(W)S_2$ active phase are presented in Table 1. W_{12}/Al_2O_3 catalyst consisted predominantly the slabs with length ~ 3.4 nm while Mo_{12}/Al_2O_3 had shorter slabs ~ 3.1 nm, in agreement with results reported in [22,34,35] showing that WS_2 particles are usually larger than MoS_2 ones. Adding one Mo atom to the catalysts with Mo/W=1/11 allowed to slightly decrease the average slab length compared to W_{12}/Al_2O_3 (from 3.4 to 3.2 nm), further increase of molybdenum content to Mo/W=3/9 resulted to decrease in the average length, from 3.4 to 2.9 nm. The average stacking number for all bimetallic catalysts was higher than that observed for monometallic references. Moreover, the stacking of catalysts prepared from a mixture of HPAs seems to be higher compared to their mixed HPAs based counterparts. These changes can be explained by altering sulfidation rates of Mo and W leading to incorporation of Mo atoms into WS_2 slabs.

However, HRTEM characterization gives general morphological information of the sulfided phase but does not allow to distinguish between MoS_2 or WS_2 slabs. Complementary analysis was thus performed by HAADF, where the Z contrast between Mo and W atoms is favorable to discriminate them. Typical HAADF images of gas sulfided $Mo(W)/Al_2O_3$ catalysts are presented

in Fig. 3 and reveal the 2D morphology of the sulfided slabs. All images of W_{12}/Al_2O_3 sample present a very homogeneous intensity of tungsten atoms in the slabs, as illustrated in Fig. 3 (a). On sulfided mixed Mo_3W_9/Al_2O_3 catalysts, differences in contrast between atoms in the slabs are observed, which can be attributed to the difference in Z between Mo and W (Fig. 3 (c)). Differences in thickness of the support cannot explain these differences as they are never observed on the pure WS_2 supported catalyst. This is confirmed by the intensity profiles in a row of atoms, where the ratio of intensity is equal to the ratio of the $Z^{1.7}$ as expected for this technique (Fig. 3 (d)). It is clearly seen that using mixed MoW HPA contributed to the formation of mixed $Mo_nW_{12-n}S_2$ particles with core-shell structure, where Mo atoms are located predominantly together in the core of the WS_2 slab. On the contrary, HAADF images of Mo_3+W_9/Al_2O_3 catalyst prepared from two separate HPAs show a large majority of monometallic MoS_2 and WS_2 slabs with only few bimetallic particles (Fig. 3 (b)).

3.1.3 Catalytic activities in co-HDT of DBT and naphthalene after activation under H_2/H_2S

The catalytic activities of the Mo_nW_{12-n}/Al_2O_3 catalysts sulfided under H_2/H_2S in HDS of DBT and HYD of naphthalene are presented in Table 5. The reactants conversions varied in a wide range, from 20.8 to 52.9 % for DBT HDS and from 23.6 to 47.8 % for naphthalene HYD over all prepared catalysts. The W_{12}/Al_2O_3 sample demonstrated the lowest activities in DBT HDS as well as in naphthalene HYD. Monometallic Mo_3W_9/Al_2O_3 and Mo_{12}/Al_2O_3 catalysts achieved the highest conversion values in DBT HDS and naphthalene HYD. Both samples Mo_1+W_{11}/Al_2O_3 and Mo_3+W_9/Al_2O_3 prepared from separate monometallic HPA demonstrated a much lower activity than their bimetallic Mo_1W_{11}/Al_2O_3 and Mo_3W_9/Al_2O_3 analogs synthesized from mixed HPAs with the same metal contents.

3.2 Comparison of characterization and performance of $Mo(W)/Al_2O_3$ catalysts after activation under gas and liquid phase

The activation of the Mo(W)/Al_2O_3 catalysts was performed by two procedures: GS in present work and LS as it was previously reported [22]. The sulfidation behavior and catalytic properties of the (Mo)W catalysts were different depending on the sulfiding agent. It should be noted that the sulfidation procedures using the different sulfidation agents were not performed under the same conditions. LS was performed by heating in hydrogen flow at 3.5 MPa with a mixture of DMDS in decane in two steps (first at 240 ºC for 10 h and second at 340 ºC for 6 h). GS activation was carried out in one step under a flow of H_2S/H_2 at atmospheric pressure and heating to 400 ºC over a holding period of 2 h. However, the HDT activity tests were performed using the same model feed (DBT and naphthalene) in identical conditions in both cases. Therefore, correct comparison of sulfidation methods (gas versus liquid phase) and its effect on the state of active phase particles determined by XPS and HRTEM as well as the morphology of mixed Mo(W)S_2 species evidenced by HAADF and the catalytic properties is possible.

3.2.1 Comparison of the morphology of the active Mo(W)S_2 phase

If we compare with the results obtained by LS [22] (Fig. 4), it can be seen that GS resulted in the formation of shorter and mainly slightly higher stacked slabs, thus after GS the average length of particles in all samples in average was 3.1 nm against 4.8 nm for LS. The most significant changes were detected for the catalysts based on a mixture of two HPAs.

The results of HAADF characterization of the liquid phase sulfided Mo(W)/Al_2O_3 catalysts were shown in [22]. One can observe that the use of mixed $SiMo_3W_9$ HPA as an initial precursor led to the formation of mixed $Mo_nW_{12-n}S_2$ particles with Mo atoms inside WS_2 slabs in both cases. However, GS was more preferable to the formation of the particles with core-shell structure, while LS one led to more randomly distribution of molybdenum inside the WS_2.

3.2.2 Comparison of the sulfidation rate of Mo(W)S_2 phase

The effect of sulfidation method on metal sulfidation degree as determined by XPS was also evaluated. The activation procedure has little effect on the sulfidation rate of monometallic and

bimetallic references catalysts with variation below 5 %. A larger difference in metal sulfidation degree (15 % for Mo and 18% for W in favor of liquid phase method) was observed for $SiMo_nW_{12-n}$ HPAs based catalysts. This can be attributed to the formation of the mixed $MoWS_2$ particles with different structure, more strongly affected by the sulfidation agent resulting in different temperatures of H_2S availability. In the case of gas sulfidation, the sulfiding agent H_2S is present from room temperature and may lead to the formation of partly sulfided intermediate at lower temperature than in the case of DMDS, which decomposition occurs at ~150 °C. We can imagine that these intermediates growth is favored under H_2S and leads to larger Mo entities than in the case of LS. In the case of GS the Mo atoms could start sulfiding at room temperature with formation of MoS_2 slabs, when tungsten disulfide appears at higher temperature and could then cover the edges of MoS_2 particle resulting in core-shell structure, in agreement with HAADF results. LS led to randomly distribution of molybdenum inside the WS_2 particle. In this case, Mo starts sulfiding at temperature of DMDS decomposition that is close to the startup sulfidation temperature of W that allows to form mixed $MoWS_2$ sulfide particles, where molybdenum atoms are more randomly distributed inside the slabs [22].

3.2.3 Comparison of activity in co-HDT of DBT and naphthalene

The catalytic activity of MoW/Al_2O_3 catalysts activated by GS and LS was examined in the model reaction of DBT HDS and naphthalene HYD in order to evaluate the influence of sulfidation method on their catalytic properties. The differences in catalytic properties of the MoW/Al_2O_3 catalysts with respect to the sulfidation procedures are shown in Fig. 5. H_2S activation of all studied samples led to higher HDS (Fig. 5 (a)) and HYD (Fig. 5 (b)) activity than the DMDS activation. Increasing of HDS activity when H_2S was used for sulfidation was reported by Gochi et al. for bulk MoWNi [24] for $CoMo/Al_2O_3$ catalysts [23,25]. Conflicting results have been reported in the literature [26] regarding unpromoted Mo/Al_2O_3.

In our case better catalytic activity of GS catalysts can be related to the shorter size of formed $Mo(W)S_2$ species compared to LS ones and, therefore, higher active sites content. However, a single size effect cannot explain all obtained catalytic properties and other factors should be considered. For example, both monometallic catalysts differed in ~ 1.5 nm of $Mo(W)S_2$ slab average length after GS (Table 1) and LS activation [22]. At the same time, its delta in catalytic activity after GS and LS sulfidation differed significantly (Fig. 5 (c)). The greatest effect of the type of sulfidation was observed for monometallic W catalyst, GS activation provides increasing DBT HDS by 9 times and naphthalene HYD by 7 times compared to the samples activated by LS. On contrary, HDS activity of molybdenum monometallic and bimetallic catalysts was increased more than 2 times after H_2S activation compared to DMDS sulfidation, while HYD activity increased ~ 2 times. However, the trend in distribution of the catalytic properties was kept whatever the activation protocol. In both cases, the catalysts prepared from the mixed HPA exhibited significantly higher activity in the two reactions than their counterparts prepared from a mixture of monometallic HPAs (Fig. 5 (c)). Moreover, Mo_3W_9/Al_2O_3, with only 3 atoms of Mo for 9 of W, showed as good performance in HDS as Mo_{12}/Al_2O_3 catalyst with the highest HYD properties of the series. The high efficiency of mixed HPAs based catalysts compared to Mo+W ones can be attributed to the presence of mixed $Mo_nW_{12-n}S_2$ active phase evidenced by HAADF being more favorable for HDS as well as HYD catalytic activity.

The selectivity of prepared catalysts toward the HYD pathway of DBT HDS was also estimated (Fig. 6). It was found that HYD pathway is more preferred for mixed HPAs based catalysts compared to their counterparts regardless of the type of sulfidation. Improved HYD properties of these catalysts can be attributed to the appearance of new mixed $Mo_nW_{12-n}S_2$ active sites after sulfidation of mixed molecular precursors. However, all catalysts activated in flow H_2S/H_2 exhibit significantly higher $S_{HYD/DDS}$ value, in agreement with the observation that DMDS activation enhances C-S hydrogenolysis [24,36]. It is interesting to note that the increment of the rate constant for the catalysts sulfided by gas mixture H_2S/H_2 linearly depended on the increase of

rate constants in naphthalene HYD (Fig. 7). It means that higher HDS activity is rather related to enhanced hydrogenation properties of the catalysts.

3.3 Catalytic activities in co-HDT of DBT, 4,6-DMDBT and naphthalene

Taken into account the beneficial effect of gas phase sulfidation on modifying the efficiency of the active sites this activation procedure was chosen for further investigation. The catalytic behavior of the synthesized (Mo)W/Al_2O_3 catalysts activated by GS was evaluated in simultaneous HDS of DBT and 4,6-DMDBT and HYD of naphthalene. The conversion of reactants is shown in Table 6. Rate constants values depending on the reaction type increased in the order 4,6-DMDBT HDS < DBT HDS < naphthalene HYD. We have never observed toluene undergoing hydrogenation under chosen reaction conditions.

Conversion of naphthalene varied from 16.2 to 34.6%. Under chosen conditions, naphthalene was transformed only into decaline over all tested catalysts. Addition of Mo to the composition of the catalysts prepared from a mixture of monometallic HPAs had no significant effect on naphthalene HYD, compared to W_{12}/Al_2O_3. On the contrary, incorporation of one Mo atom in case of Mo_1W_{11}/Al_2O_3 catalyst allowed to increase rate constants k_{HYD} from 66.7×10^5 mol h^{-1} g^{-1} to 92.2×10^5 mol h^{-1} g^{-1}, when the further increase in molybdenum content for Mo_3W_9/Al_2O_3 led to reach k_{HYD}=128.8×10^5 mol h^{-1} g^{-1}, that almost twice higher than for W_{12}/Al_2O_3 and 1.4 times more than for Mo_{12}/Al_2O_3. As consequence, both mixed HPAs based samples demonstrated higher HYD activity than their analogs.

It can be seen that DBT conversion over (Mo)W/Al_2O_3 catalysts changed from 14.3 to 36.6 %, and for 4,6-DMDBT from 22.7 to 64.2 %. As in the case of naphthalene HYD, the use of a mixture of HPAs for catalysts preparation did not give any beneficial effect in HDS of DBT as well 4,6-DMDBT. While substitution of one tungsten atom to molybdenum into SiW_{12} HPA led to increase HDS activity at least 1.6 times compared to W_{12}/Al_2O_3. The use of $SiMo_3W_9$ HPA resulted in the increase of $k_{HDS\ DBT}$ from 2.7×10^5 mol h^{-1} g^{-1} to 27.7×10^5 mol h^{-1} g^{-1} and $k_{HDS\ 4,6-}$

$_{DMDBT}$ from 4.0×10^5 mol h^{-1} g^{-1} to 12.6×10^5 mol h^{-1} g^{-1}. At the same time, Mo_3W_9/Al_2O_3 had demonstrated significantly better activity in all evaluated reactions compared to Mo_{12}/Al_2O_3. As previously, both mixed HPAs based catalysts had higher HDS catalytic activity than their counterparts with the same Mo/W ratio.

The changes in the size and stacking number of active phase particles as well as in sulfidation degree in bimetallic catalysts cannot explain the changes in catalytic properties. It can be concluded that the MoW nanoscale proximity in the structure of mixed HPAs resulting in the formation of mixed $Mo_nW_{12-n}S_2$ active phase particles with core-shell structure, is at the origin of higher catalytic activity of the mixed HPAs based catalysts.

Cyclic sulfur compounds as DBT and 4,6-DMDBT react through two pathways: DDS and HYD during HDS reactions. The selectivity ratios $S_{HYD/DDS}$ in HDS reactions of all catalysts were calculated and shown in Table 6. All prepared catalysts had high selectivity in respect of hydrogenation pathway of HDS. Nevertheless, Mo_{12}/Al_2O_3 as it was expected, demonstrated the lowest $S_{HYD/DDS}$ in HDS of both DBT and 4,6-DMDBT. Fig. 8 shows a dependence of 4,6-DMDBT conversion and corresponding selectivity ratios on the nature of starting precursor. The mixed HPAs based catalysts presented higher selectivity ratios than those obtained for their bimetallic counterparts. In addition, the Mo_3W_9/Al_2O_3 catalyst had the highest 4,6-DMDBT HYD/DDS selectivity ratio. This observation supports the formation of mixed $MoWS_2$ active sites developing strong hydrogenation properties required for the treatment of refractory sulfur compounds.

In addition, for a better understanding of the beneficial role of mixed MoW HPAs the rate constants of HDS and HYD reactions over bimetallic catalysts were calculated by the additive way using the values for monometallic catalysts Mo_{12}/Al_2O_3 and W_{12}/Al_2O_3 and necessary Mo/W proportions (Table 6). Thus, bimetallic catalysts prepared by using mixed $SiMo_nW_{12-n}$ HPAs had higher experimental values of the rate constant in all studied reactions than predicted ones. In contrast, the experimental data for the samples prepared by using a mixture of two monometallic

HPAs resulted from the linear combination of the two monometallic references or even lower in case of Mo_1+W_{11}/Al_2O_3.

Relative HDS activity (normalized on HDS rate constants on Mo_{12}/Al_2O_3) was also calculated for DBT and 4,6-DMDBT HDS (Fig. 9). Relative HDS activity of Mo_3W_9/Al_2O_3 catalyst was close to monometallic Mo_{12}/Al_2O_3 one in DBT HDS. Other Mo-W catalysts had lower activity compared to Mo_{12}/Al_2O_3 reference. In contrast, in 4,6-DMDBT reaction, all Mo-W catalysts have higher relative HDS activity or similar (Mo_1+W_{11}/Al_2O_3) than monometallic ones (Mo_{12}/Al_2O_3 or W_{12}/Al_2O_3). It is clearly seen that Mo-W synergetic effect is much higher in 4,6-DMDBT HDS compared to DBT HDS performance. This effect is related with different mechanisms between HDS of DBT and highly refractory 4,6-DMDBT due to the steric hindrance of the methyl groups at the 4- and 6 positions.

4. Conclusions

In summary, the main results of the work are as follows:

1. It was found that with the increase of Mo content in all bimetallic MoW/Al_2O_3 catalysts synthesized by using mixed $SiMo_1W_{11}$ and $SiMo_3W_9$ HPAs, the increase of W sulfidation degree occurs compared to the monometallic W_{12}/Al_2O_3 catalyst. In addition, this Mo incorporation into the bimetallic catalysts resulted in a decrease of the average slab length of $(Mo)WS_2$ species after gas phase sulfidation.
2. Using HAADF it was demonstrated that gas phase sulfidation of mixed molecular precursor led to formation of a core-shell structure, where Mo was mostly located in the core and W in the shell. In contrast, Mo_3+W_9/Al_2O_3 catalyst prepared from two $SiMo_{12}$ and SiW_{12} HPAs (with Mo/W ratio in the catalyst equal to 3/9) show a large majority of monometallic MoS_2 and WS_2 slabs with only few bimetallic particles.
3. $Mo(W)/Al_2O_3$ catalysts, which were sulfided by GS, demonstrated higher activity in DBT HDS as well as naphthalene HYD compared to the analogs activated by LS. GS led to formation a

shorter Mo(W)S_2 crystallites with core-shell structure having significant HYD activity as evidenced by higher DBT HDS selectivity ratio $S_{HYD/DDS}$ and naphthalene HYD than the catalysts, which have been undergone LS, having Mo(W)S_2 species with randomly distribution of molybdenum inside the WS_2.

4. Catalytic results in HDS and HYD reactions clearly demonstrated that catalysts prepared from mixed MoW HPAs are much more active than their counterparts prepared from a mixture of monometallic HPAs. Moreover, Mo_3W_9/Al_2O_3 with only 3 atoms of Mo for 9 of W showed better performance in HDS and HYD than Mo_{12}/Al_2O_3 catalyst. Mo-W core-shell synergetic effect is much higher in 4,6-DMDBT HDS compared to DBT HDS performance. In addition, mixed HPAs based catalysts had the highest selectivity in respect of HYD pathway in 4,6-DMDBT HDS.

Acknowledgments

The research was financial supported by the Ministry of Education and Science of the Russian Federation, project No. 14.586.21.0054 (unique identifier of project RFMEFI58617X0054) and The Ministry of Foreign Affairs and International Development (France) and the Ministry of National Education, Higher Education and Research (France) in framework of PHC Kolmogorov Programme 2017-2019. M. Nikulshina thanks French Ambassy in Russia for the Vernadsky fellowship and Haldor Topsøe Company for the grant to perform her PhD thesis. Chevreul Institute (FR 2638), Ministère de l'Enseignement Supérieur et de la Recherche, Région Nord – Pas de Calais and FEDER are acknowledged for supporting and funding partially this work.

References

[1] X. Ma, K. Sakanishi, I. Mochida, Ind. Eng. Chem. Res. 33 (1994) 218–222.

[2] V. Meille, E. Schulz, M. Lemaire, M. Vrinat, J. Catal. 170 (1997) 29–36.

[3] X.-L. Ma, K. Sakaanishi, I. Mochida, Ind. Eng. Chem. Res. 35 (1996) 2487–2494.

[4] S. Eijsbouts, F. Plantenga, B. Leliveld, Y. Inoue, K. Fujita, Prepr. Pap.-Am. Chem. Soc. Div. Fuel Chem. 48 (2) (2003) 494–495.

[5] C. Thomazeau, C. Geantet, M. Lacroix, M. Danot, V. Harle, Oil gas sci. technol. 60 (2005) 781-790.

[6] C. Thomazeau, C. Geantet, M. Lacroix, V. Harle, S. Benazeth, C. Marhic, A M. Danot, J. Solid State Chem. 160 (2001) 147-155.

[7] C. Yin, H. Liu, L. Zhao, B. Liu, S. Xue, N. Shen, Y. Liu,Y. Li, C. Liu, Catal. Today. 259 (2016) 409–416.

[8] L. Wang, Y. Zhang, Y. Zhang, Z. Jiang, C. Li, Chem. Eur. J. 15 (2009) 12571–12575.

[9] S. Sigurdson, V. Sundaramurthy, A.K. Dalai, J. Adjaye, J. Mol. Catal. A: Chem. 291 (2008) 30–37.

[10] J. A. Mendoza-Nieto, O. Vera-Vallejo, L. Escobar-Alarcón, D. Solís-Casados, T. Klimova, Fuel. 110 (2013) 268–277.

[11] P. Nikulshin, A. Mozhaev, C. Lancelot, P. Blanchard, E. Payen, C. Lamonier, C. R. Chimie 19 (2016) 1276-1285.

[12] R. Shafi, M.R.H. Siddiqui, G.J. Hutchings, E.G.I.V. Derouane, Kozhevnikov, Appl. Catal. A. 204 (2000) 251–256.

[13] B. Pawelec, R. Mariscal, J.L.G. Fierro, A. Greenwood, P.T. Vasudevan, Appl. Catal. A. 206 (2001) 295–307.

[14] P. Blanchard, C. Lamonier, A. Griboval, E. Payen, Appl. Catal. A. 322 (2007) 33–45.

[15] P.A. Nikulshin, N.N. Tomina, A.A. Pimerzin, A.V. Kucherov, V.M. Kogan, Catal. Today. 149 (2010) 82–90.

[16] P.A. Nikulshin, N.N. Tomina, A.A. Pimerzin, A.Yu. Stakheev, I.S. Mashkovsky, V.M. Kogan, Appl. Catal. A. 393 (2011) 146–152.

[17] C.I. Cabello, F.M. Cabrerizo, A. Alvarez, H.J. Thomas, J. Mol. Catal. A: Chem. 186 (2002) 89–100.

[18] C. Lamonier, C. Martin, J. Mazurelle, V. Harlé, D. Guillaume, E. Payen, Appl. Catal. B. 70 (2007) 548–556.

[19] A. Griboval, P. Blanchard, E. Payen, M. Fournier, J.L. Dubois, Catal. Today. 45 (1998) 277–283.

[20] L. Lizama, T. Klimova. L. Lizama, T. Klimova, Appl. Catal. B. 82 (2008) 139–150.

[21] N.N. Tomina, P.A. Nikul'shin, A.A. Pimerzin, Pet. Chem. 48 (2) (2008) 92–99.

[22] M. Nikulshina, A. Mozhaev, C. Lancelot, M. Marinova, P. Blanchard, E. Payen, C. Lamonier, P. Nikulshin, Appl. Catal. B. 224 (2018) 951–959.

[23] R. Prada Silvy, F. Delannay, P. Grange and B. Delmon, Appl. Catal., 46 (1989) 113-129.

[24] Y. Gochi, C. Ornelas, F. Paraguay, S. Fuentes, L. Alvarez, J.L. Rico, G. Alonso-Núñez, Catal. Today. 107–108 (2005) 531–536.

[25] P.A. Nikulshin, A.V. Mozhaev, K.I. Maslakov, A.A. Pimerzin, V.M. Kogan, Appl. Catal. B. 158–159 (2014) 161–174.

[26] S. Texier, G. Berhault, G. Pérot, V. Harlé, F. Diehl, J. Catal. 223 (2004) 404–418.

[27] L. van Haandel, M. Bremmer, P.J. Kooyman, J.A.R. van Veen, T. Weber, E.J.M. Hensen, ACS Catal. 5 (2015) 7276–7287.

[28] S. Kasztelan, H. Toulhoat, J. Grimblot, J.P. Bonnelle, Appl. Catal. 13 (1984) 127–159.

[29] P.A. Nikulshin, A.V. Mozhaev, K.I. Maslakov, A.A. Pimerzin, V.M. Kogan, Appl. Catal. B. 158-159 (2014) 161–174.

[30] P.P. Minaev, P.A. Nikulshin, M.S. Kulikova, A.A. Pimerzin, V.M. Kogan, Appl. Catal. A. 505 (2015) 456–466.

[31] A.V. Mozhaev, P.A. Nikulshin, Al.A. Pimerzin, K.I. Maslakov, A.A. Pimerzin, Catal. Today. 271 (2016) 80–90.

[32] A. Cordova, P. Blanchard, C. Lancelot, G. Frémy, C. Lamonier, ACS Catal. 5 (2015) 2966–2981.

[33] A. Cordova, P. Blanchard, H. Salembier, C. Lancelot, G. Frémy, C. Lamonier, Catal. Tod. 292 (2016) 143–153.

[34] D. Ishutenko, P. Nikulshin, A. Pimerzin, Catal. Today. 271 (2016) 16–27.

[35] D. Ishutenko, P. Minaev, Yu. Anashkin, M. Nikulshina, A. Mozhaev, K. Maslakov, P. Nikulshin, Appl. Catal. B. 203 (2017) 237–246.

[36] J. Vangestel, J.Leglise, J.C. Duchet, J. Catal. 145 (1994) 429–436.

Captions for Figures

Figure 1. The examples of decomposition od W 4f (a), Mo 3d (b) and S 2p (c) photoelectron spectra recorded for Mo_3W_9/Al_2O_3 catalyst (For interpretation of the references to color in this figure legend, the reader is referred to the web version of the article).

Figure 2. HRTEM micrographs of gas sulfided $Mo(W)/Al_2O_3$ catalysts.

Figure 3. HAADF images of sulfided W_{12}/Al_2O_3 (a), Mo_3+W_9/Al_2O_3 (b), Mo_3W_9/Al_2O_3 (c) catalysts with intensity profiles (d) corresponding to the row of atoms identified by the arrow on Mo_3W_9/Al_2O_3.

Figure 4. Average length (a) and average stacking number (b) of the $Mo(W)S_2$ crystallites in gas and liquid sulfided $Mo(W/)Al_2O_3$ catalysts.

Figure 5. Rate constants of DBT HDS (a) and naphthalene HYD (b) over $Mo(W)/Al_2O_3$ catalysts using GS and LS sulfidation procedures and dependence between DBT HDS rate constants (c).

Figure 6. Changing the selectivity ratio $S_{HYD/DDS}$ in DBT HDS depending on of the sulfidation method.

Figure 7. Dependence of DBT HDS rate constants ratio of the catalysts after gas (GS) and liquid (LS) sulfidation vs naphthalene HYD ratio.

Figure 8. Relationship between conversion of 4,6-DMDBT and the selectivity ratio $S_{HYD/DDS}$ on $Mo(W)/Al_2O_3$ catalysts.

Figure 9. Relative HDS activity of $Mo(W)/Al_2O_3$ catalysts in DBT and 4,6-DMDBT HDS (filled columns correspond to catalysts prepared from one precursor: Mo_{12}, W_{12}, Mo_1W_{11} and Mo_3W_9 HPA; empty columns correspond to catalysts prepared from mixtures of Mo_{12} and W_{12} HPA with 1/11 and 3/9 stoichiometry of Mo/W).

Captions for Tables

Table 1. Composition of prepared (Mo)W/Al_2O_3 catalysts, morphological characteristics of the (Mo)WS_2 active phase species obtained via GS and calculated from TEM micrographs.

Table 2. XPS parameters used for the decomposition of S2p and Mo3d spectra of sulfided MoW/Al_2O_3 catalysts.

Table 3. XPS parameters used for the decomposition of W4f spectra of sulfided MoW/Al_2O_3 catalysts.

Table 4. Relative metal fractions measured by XPS for molybdenum and tungsten species present at the surface of Mo(W)/Al_2O_3 catalysts after gas phase (GS) and liquid phase (LS) sulfidation.

Table 5. Catalytic properties of prepared (Mo)W/Al_2O_3 catalysts sulfided in gas phase in HDT of a mixture of DBT and naphthalene.

Table 6. Catalytic properties of prepared (Mo)W/Al_2O_3 catalysts sulfided in gas phase in HDT of a mixture of DBT, naphthalene and 4,6-DMDBT.

Table 1

Composition of prepared (Mo)W/Al_2O_3 catalysts, morphological characteristics of the (Mo)WS_2 active phase species obtained via GS and calculated from HRTEM micrographs.

Catalyst	Composition (wt. %)		Characteristics of (Mo)WS_2 slabs from HRTEM statistics		Distribution of slab length (rel. %)					Distribution of stacking number (rel. %)			
	Mo	W	Average length $\bar{L}$ (nm)	Average stacking number $\overline{N}$	<2 (nm)	2-4 (nm)	4-6 (nm)	6-8 (nm)	>8 (nm)	1	2	3	>3
Mo_{12}/Al_2O_3	12.0	-	3.1	1.4	14	65	17	3	1	70	24	5	1
W_{12}/Al_2O_3	-	20.8	3.4	1.4	13	60	20	5	2	66	28	4	2
Mo_1W_{11}/Al_2O_3	0.9	19.2	3.2	1.9	21	57	17	4	1	45	33	13	9
Mo_3W_9/Al_2O_3	2.8	15.9	2.9	1.7	35	45	16	3	1	52	35	9	4
Mo_1+W_{11}/Al_2O_3	0.9	19.2	3.1	2.0	24	58	10	6	2	38	39	14	9
Mo_3+W_9/Al_2O_3	2.8	15.9	2.9	2.1	23	63	11	2	1	42	26	19	13

Table 2

XPS parameters used for the decomposition of S2p and Mo3d spectra of sulfided MoW/Al_2O_3 catalysts.

Species	Peak	Constraint Area	Constraint FWHM	Constraint BE (eV)
S^{2-}	$S2p_{3/2}$ (A)	A	[a]A = $FWHM_{Al2p} \times 0.91$ (±0.1 eV)	[c]A = 162.3 ; 161.3
	$S2p_{1/2}$	A × 0.5	A × 1.1	A + 1.2
S_2^{2-}	$S2p_{3/2}$ (B)	B	A × 1	B = 163.5 ; 162.7
	$S2p_{1/2}$	B × 0.5	A × 1.1	B + 1.2
S^{2-}	S2s (C)	C = (1.5×A)/1.4 ; (1.5×A)/1.3	[b]C = A × 1.77 (±0.1 eV)	C = (A+65) ; (A+64)
S_2^{2-}	S2s (D)	D = (1.5×B)/1.4 ; (1.5×B)/1.3	C × 1	D = (B+65) ; (B+64)
Mo^{IV} (MoS_2)	Mo $3d_{5/2}$ (E)	E	[a]E = $FWHM_{Al2p} \times 0.77$ (±0.1 eV)	E = 229.2 ; 228.7
	Mo $3d_{3/2}$	E × 0.67	E × 1.05	E + 3.15
Mo^{V} (Mo^{V}-OS)	Mo $3d_{5/2}$ (F)	F	[a]F = $FWHM_{Al\ 2p} \times 0.92$ (±0.1 eV)	F = 231.3 ; 230.1
	Mo $3d_{3/2}$	F × 0.67	F × 1.05	F + 3.15
Mo^{VI} (Mo^{VI}-O)	Mo $3d_{5/2}$ (G)	G	[a]G = $FWHM_{Al\ 2p} \times 1.15$ (±0.1 eV)	G = 233.2; 232.4
	Mo $3d_{3/2}$	G × 0.67	G × 1.05	G + 3.15

[a] The FWHM constraints (A, E, F, G) regarding $S2p_{3/2}$ and $Mo3d_{5/2}$ are obtained from experimental data using the FWHM of Al2p as reference.

[b] The FWHM constraint (C) regarding S2s is obtained from experimental data using the FWHM of $S2p_{3/2}$ as reference.

[c] e.g. "A = 162.3 ; 161.3" means that the value of BE can only evolve during the fit between 161.3 and 162.3 eV.

Table 3

XPS parameters used for the decomposition of W4f spectra of sulfided MoW/Al_2O_3 catalysts.

Species	Peak	Constraint Area	Constraint FWHM	Constraint BE (eV)
W^{IV}	W $4f_{7/2}$ (H)	H	[a]H= $FWHM_{Al2p} \times 0.76$ (±0.1 eV)	[b]H = 32.6 ; 32
(WS_2)	$W_{4f5/2}$	H × 0.79	H × 1.05	H + 2.15
W^{V}	W $4f_{7/2}$ (I)	I	[a]I= $FWHM_{Al2p} \times 0.92$ (±0.1 eV)	I = 34 ; 33.3
(W^{V}-OS)	$W_{4f5/2}$	I × 0.79	I × 1.05	I + 2.15
W^{VI}	W $4f_{7/2}$ (J)	J	[a]J= $FWHM_{Al2p} \times 0.97$ (±0.1 eV)	J = 36.5 ; 35.5
(W^{VI}-O)	$W_{4f5/2}$	J × 0.79	J × 1.05	J + 2.15
W^{IV} (WS_2)	W $5p_{3/2}$ (K)	H × 0.082	H × 1.37	H + 5.85
W^{V} (W^{V}-OS)	W $5p_{3/2}$ (L)	I × 0.082	I × 1.37	I + 5.85
W^{VI} (W^{VI}-O)	W $5p_{3/2}$ (M)	J × 0.082	J × 1.37	J + 5.85
Mo^{IV} (MoS_2)	Mo 4p (N)	[c]N = E × 0.165 (±5%)	[c]N = E × 2 (±0.1 eV)	[c]N = E – 192.25 (±0.2 eV)
Mo^{V} (Mo^{V}-OS)	Mo 4p (O)	[c]O = F × 0.165 (±5%)	[c]O = F × 2 (±0.1 eV)	[c]O = F - 192.25 (±0.2 eV)
Mo^{VI} (Mo^{VI}-O)	Mo 4p (P)	[c]P = G × 0.165 (±5%)	[c]P = G × 2 (±0.1 eV)	[c]P = G - 192.25 (±0.2 eV)

[a] The FWHM constraints (H, I, J) regarding W$4f_{7/2}$ are obtained from experimental data using the FWHM of Al2p as reference.

[b] e.g. "H = 32.6 ; 32" means that the value of BE can only evolve during the fit between 32 and 32.6 eV.

[c] FWHM, area and BE constraints regarding Mo4p (N, O, P) are obtained from experimental data using the FWHM of Mo$3d_{5/2}$ as reference (E, F, G in Table 2).

Table 4

Relative metal fractions measured by XPS for molybdenum and tungsten species present at the surface of Mo(W)/Al_2O_3 catalysts after gas phase (GS) and liquid phase (LS) sulfidation.

Catalyst	Mo fraction (rel. %)			W fraction (rel. %)		
	MoS_2	Mo^{V}-OS	Mo^{VI}-O	WS_2	W^{V}-OS	W^{VI}-O
Mo_{12}/Al_2O_3 GS	81	13	6	-	-	-
W_{12}/Al_2O_3 GS	-	-	-	51	16	33
Mo_1W_{11}/Al_2O_3 GS	85	13	2	51	7	42
Mo_3W_9/Al_2O_3 GS	81	14	5	64	18	18
Mo_1+W_{11}/Al_2O_3 GS	89	2	9	57	8	35
Mo_3+W_9/Al_2O_3 GS	90	8	2	77	11	12
Mo_{12}/Al_2O_3 LS	80	12	8	-	-	-
W_{12}/Al_2O_3 LS	-	-	-	56	12	32
Mo_1W_{11}/Al_2O_3 LS	100	-	-	70	11	19
Mo_3W_9/Al_2O_3 LS	96	4	-	82	5	13
Mo_1+W_{11}/Al_2O_3 LS	85	13	2	76	5	19
Mo_3+W_9/Al_2O_3 LS	88	7	5	74	8	18

Table 5

Catalytic properties of prepared (Mo)W/Al_2O_3 catalysts sulfided in gas phase in HDT of a mixture of DBT and naphthalene.

Catalyst	Conversion (%)		Selectivity ratio	Rate constants ($\times 10^5$ mol h^{-1} g^{-1})	
	DBT HDS	Naphthalene HYD	$S_{HYD/DDS}$	k_{HDS}	k_{HYD}
Mo_{12}/Al_2O_3	52.3	40.5	1.7	45.1	157.3
W_{12}/Al_2O_3	22.8	23.6	2.3	15.7	81.8
Mo_1W_{11}/Al_2O_3	49.7	42.7	2.6	41.8	168.6
Mo_3W_9/Al_2O_3	52.9	47.8	3.2	45.9	196.8
Mo_1+W_{11}/Al_2O_3	20.8	24.4	2.2	14.2	85.0
Mo_3+W_9/Al_2O_3	32.8	27.3	1.8	24.1	96.6

Table 6

Catalytic properties of prepared (Mo)W/Al_2O_3 catalysts sulfided in gas phase in HDT of a mixture of DBT, naphthalene and 4,6-DMDBT.

Catalyst	Conversion (%)			DBT HDS Selectivity ratio	4,6-DMDBT HDS Selectivity ratio	Rate constants ($\times 10^5$ mol h^{-1} g^{-1})		
	DBT HDS	Naphthalene HYD	4,6-DMDBT HDS	$S_{HYD/DDS}$	$S_{HYD/DDS}$	$k_{HDS\ DBT}$	k_{HYD}	$k_{HDS\ 4,6\text{-}DMDBT}$
Mo_{12}/Al_2O_3	33.2	26.8	22.7	1.3	2.2	24.6	94.7	3.2
W_{12}/Al_2O_3	18.9	19.8	27.9	2.3	2.9	12.7	66.7	4.0
Mo_1W_{11}/Al_2O_3	28.3	26.2	45.0	1.9	4.8	20.3 (13.7)*	92.2 (69.1)*	7.3 (3.9)*
Mo_3W_9/Al_2O_3	36.6	34.6	64.2	2.7	5.9	27.7 (15.7)*	128.8 (73.7)*	12.6 (3.8)*
Mo_1+W_{11}/Al_2O_3	14.3	16.2	28.4	1.7	3.2	9.4 (13.7)*	53.6 (69.1)*	4.1 (3.9)*
Mo_3+W_9/Al_2O_3	26.1	22.9	33.3	1.5	3.3	18.4 (15.7)*	78.8(73.7)*	5.0 (3.8)*

*The additive quantities, which were calculated using the values for bimetallic Mo_{12}/Al_2O_3 and W_{12}/Al_2O_3.

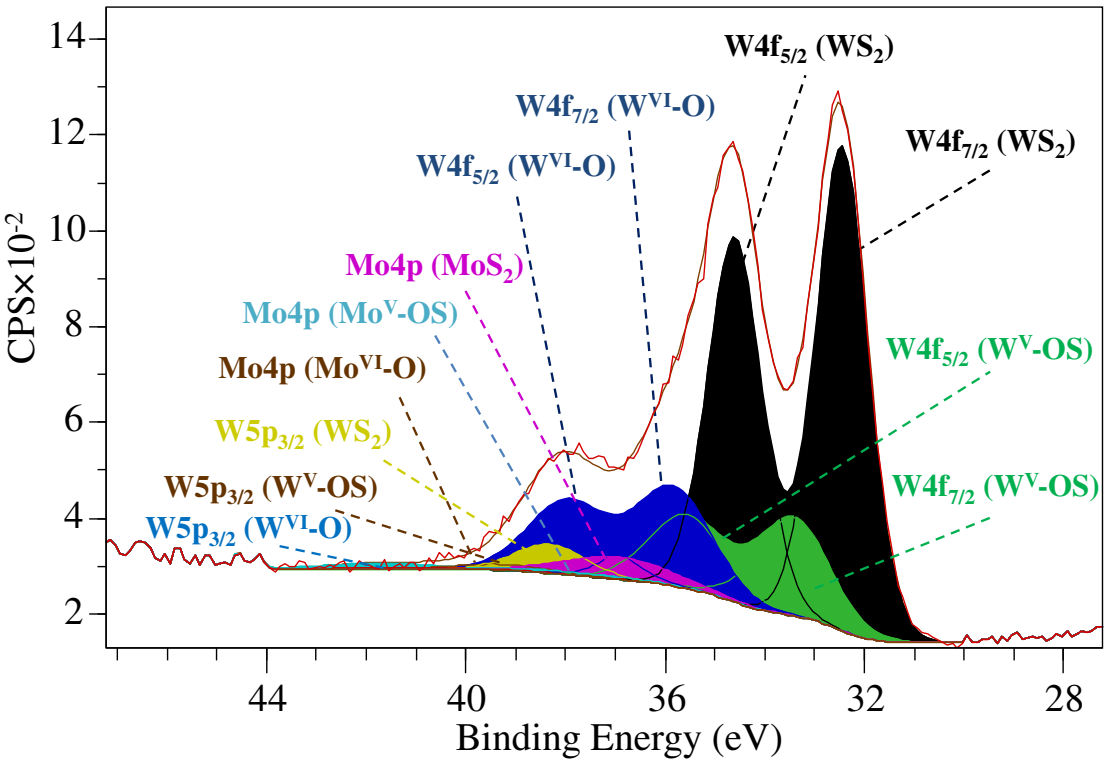
W4f5/2 (WS2)
W4f7/2 (WVI-O)
W4f5/2 (WVI-O)
W4f7/2 (WS2)
Mo4p (MoS2)
Mo4p (MoV-OS)
Mo4p (MoVI-O)
W4f5/2 (WV-OS)
W5p3/2 (WS2)
W5p3/2 (WV-OS)
W4f7/2 (WV-OS)
W5p3/2 (WVI-O)
CPS×10-2
Binding Energy (eV)

(a)

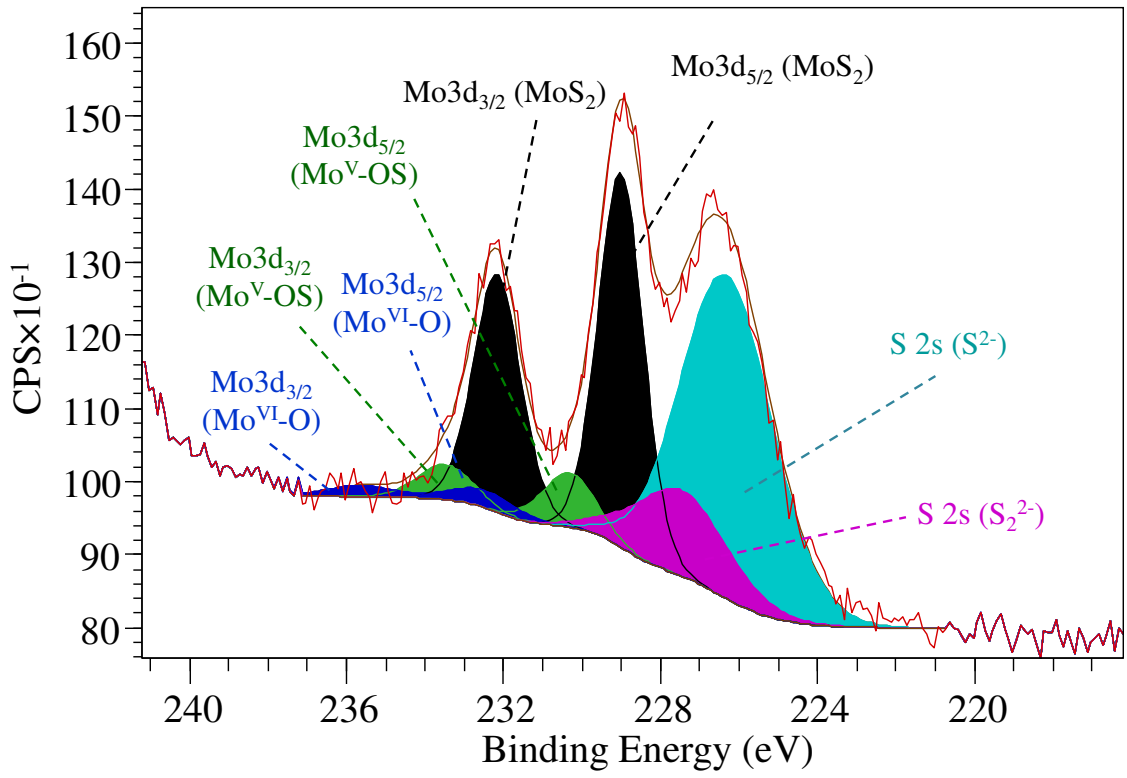
Mo3d5/2 (MoS2)
Mo3d3/2 (MoS2)
Mo3d5/2 (MoV-OS)
Mo3d3/2 (MoV-OS)
Mo3d5/2 (MoVI-O)
Mo3d3/2 (MoVI-O)
S 2s (S2-)
S 2s (S22-)
CPS×10-1
Binding Energy (eV)

(b)

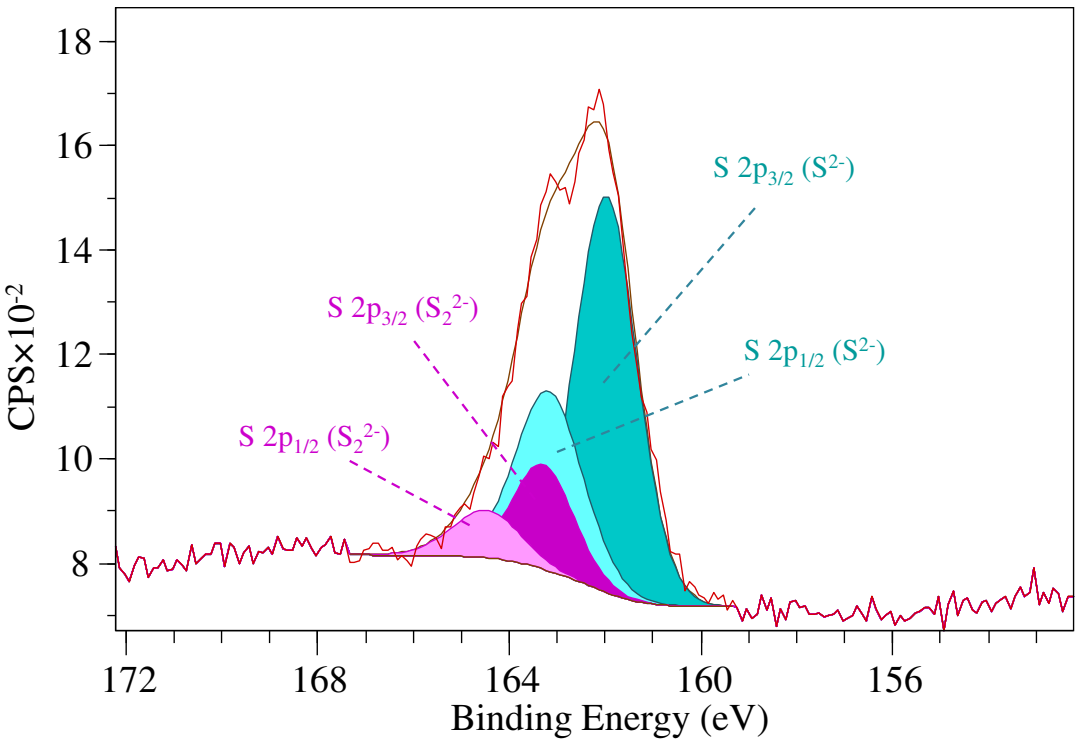

(c)

Fig. 1. The examples of decomposition od W 4f (a), Mo 3d (b) and S 2p (c) photoelectron spectra recorded for Mo_3W_9/Al_2O_3 catalyst (For interpretation of the references to color in this figure legend, the reader is referred to the web version of the article).

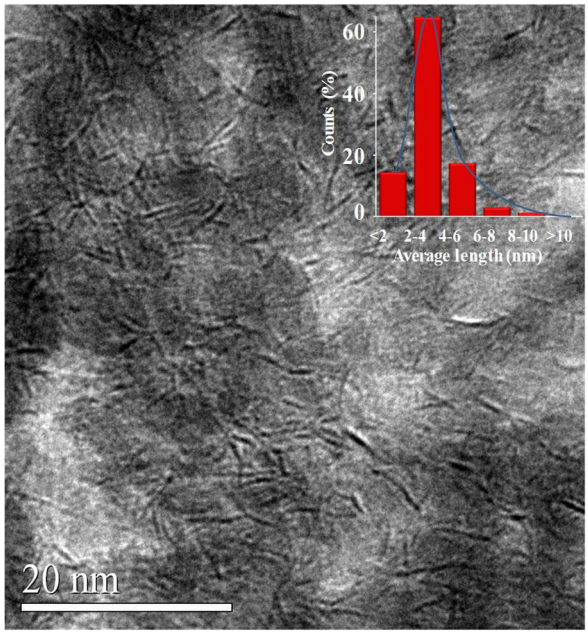

Mo_{12}/Al_2O_3

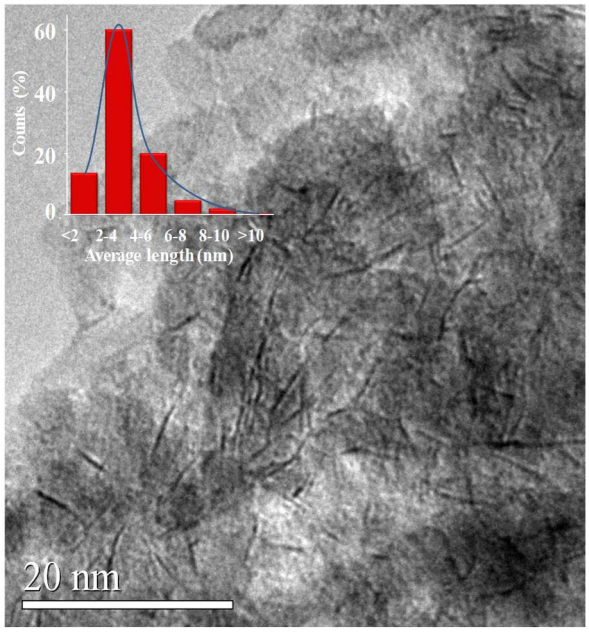

W_{12}/Al_2O_3

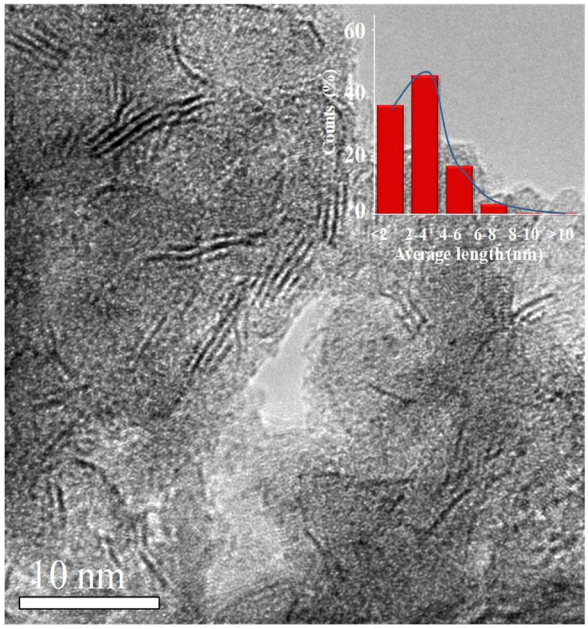

Mo_3W_9/Al_2O_3

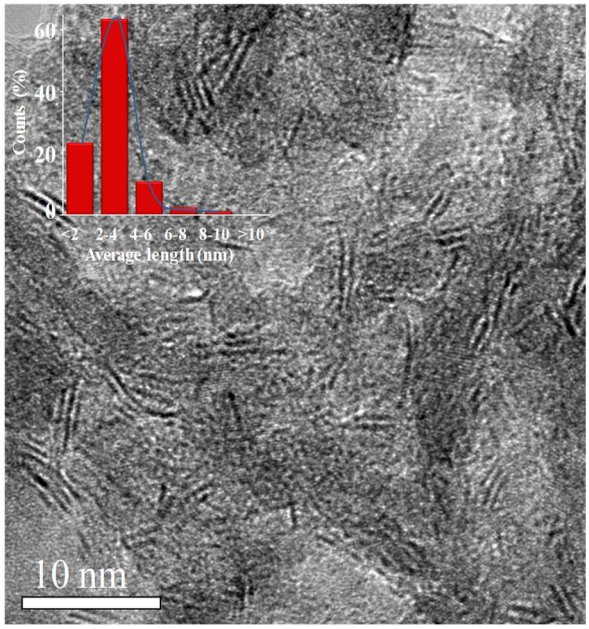

Mo_3+W_9/Al_2O_3

Fig. 2. HRTEM micrographs of gas sulfided Mo(W)/Al_2O_3 catalysts.

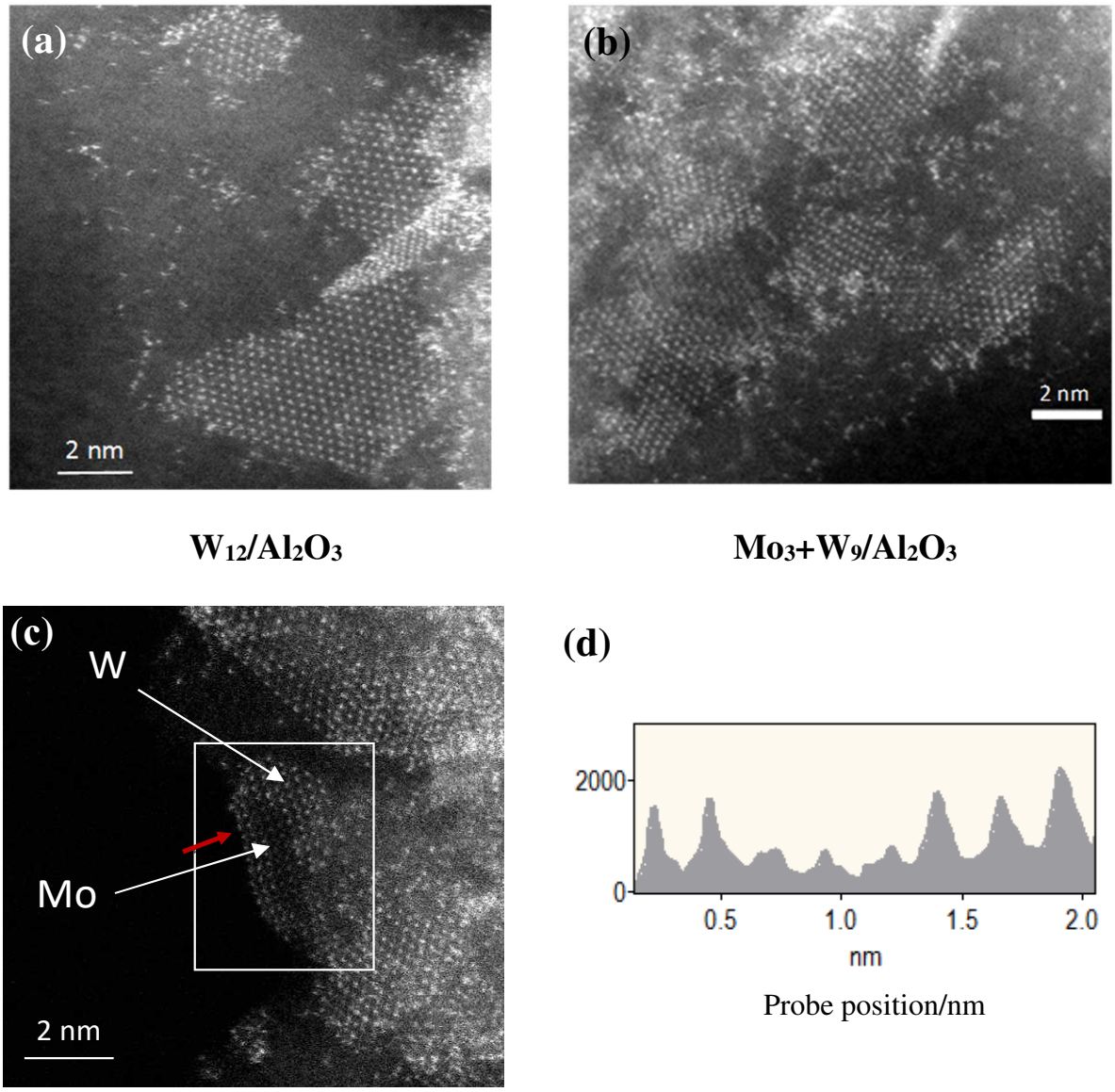

Fig. 3. HAADF images of sulfided W_{12}/Al_2O_3 (a), Mo_3+W_9/Al_2O_3 (b), Mo_3W_9/Al_2O_3 (c) catalysts with intensity profiles (d) corresponding to the row of atoms identified by the arrow on Mo_3W_9/Al_2O_3.

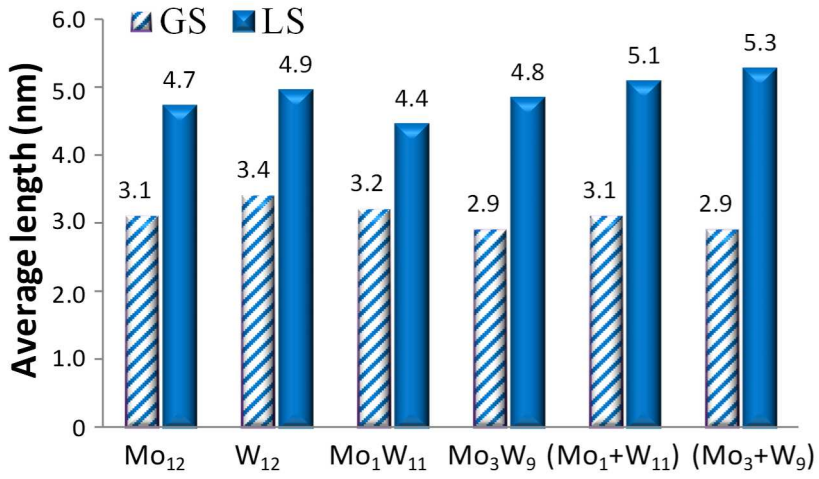

(a)

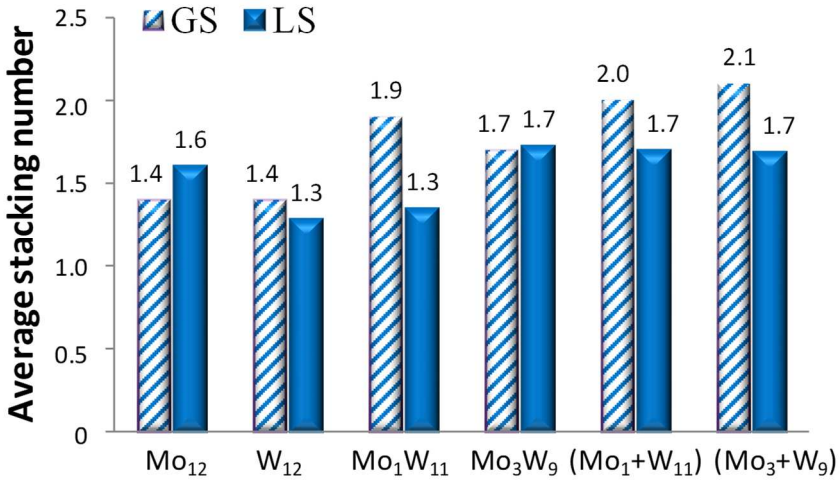

(b)

Fig. 4. Average length (a) and average stacking number (b) of the Mo(W)S_2 crystallites in gas and liquid sulfided Mo(W/)Al_2O_3 catalysts.

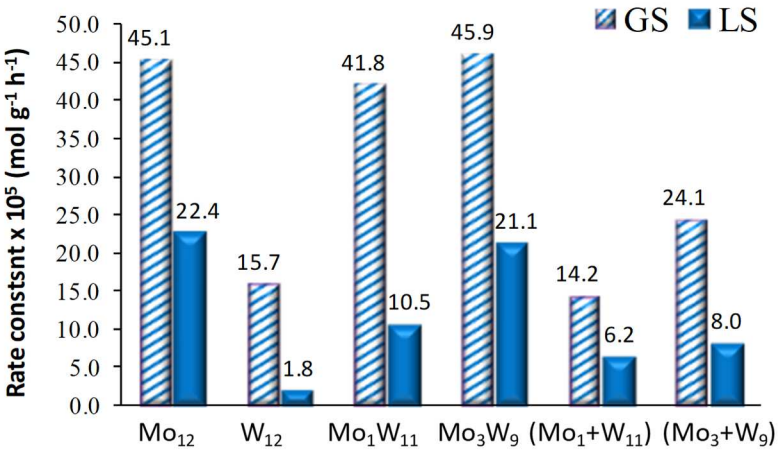

(a)

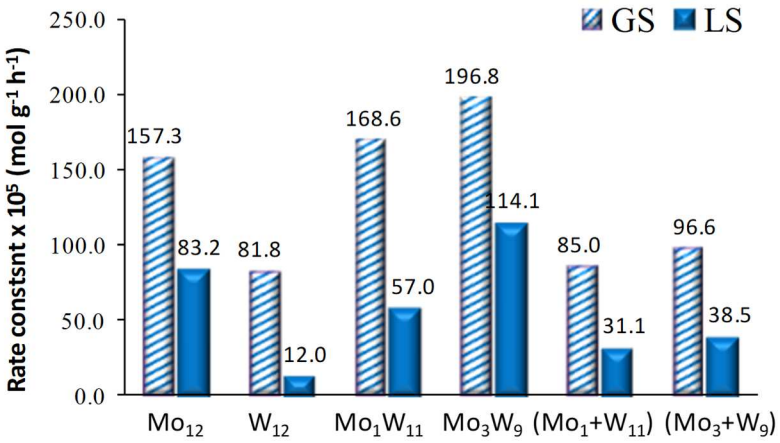

(b)

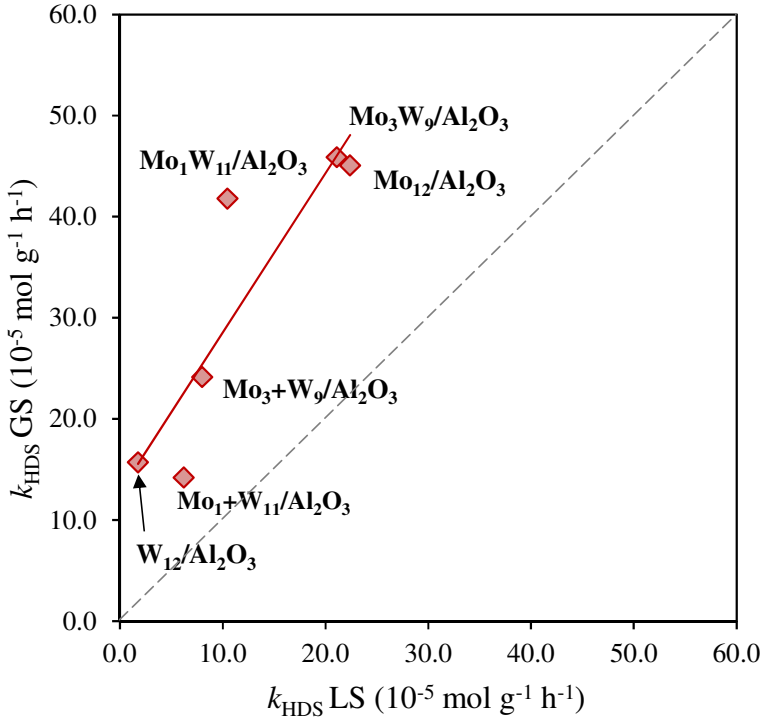

(c)

Fig. 5. Rate constants of DBT HDS (a) and naphthalene HYD (b) over Mo(W)/Al_2O_3 catalysts using GS and LS sulfidation procedures and dependence between DBT HDS rate constants (c).

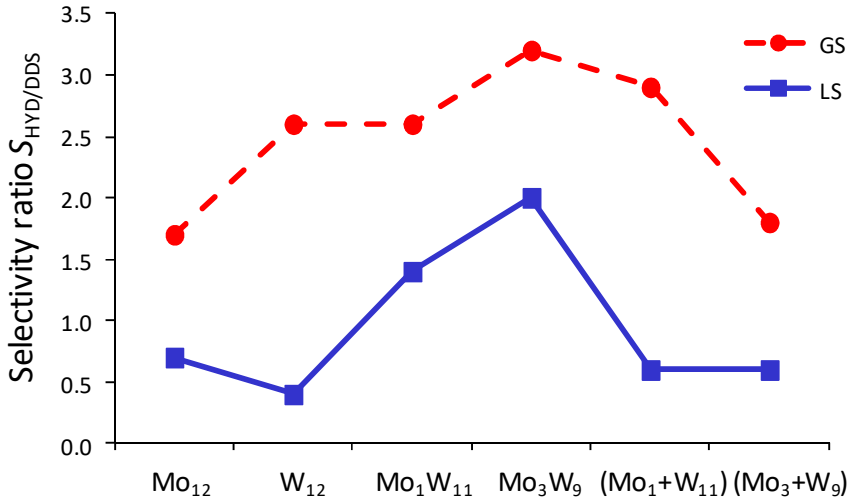

Fig. 6. Changing the selectivity ratio $S_{HYD/DDS}$ in DBT HDS depending on of the sulfidation method.

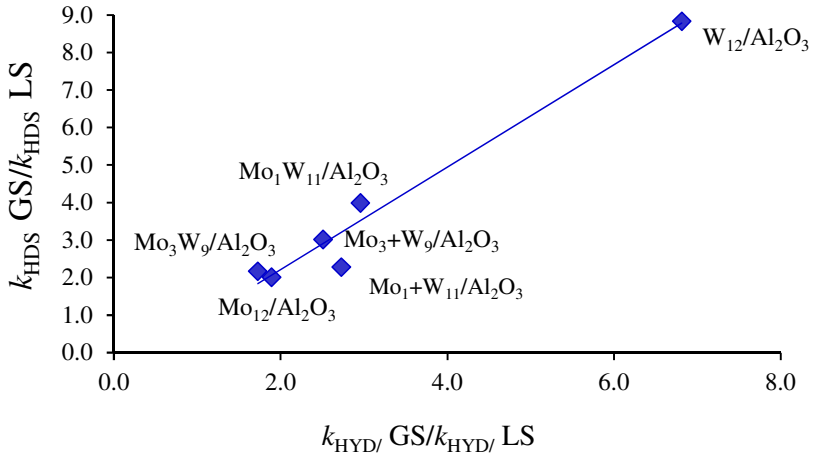

Fig. 7. Dependence of DBT HDS rate constants ratio of the catalysts after gas (GS) and liquid (LS) sulfidation vs naphthalene HYD ratio.

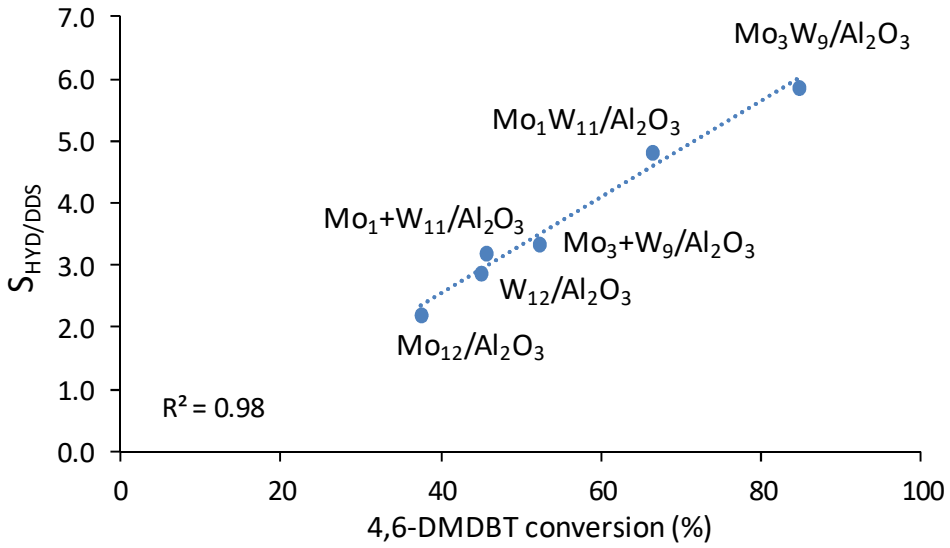

Fig. 8. Relationship between conversion of 4,6-DMDBT and the selectivity ratio $S_{HYD/DDS}$ on Mo(W)/Al_2O_3 catalysts.

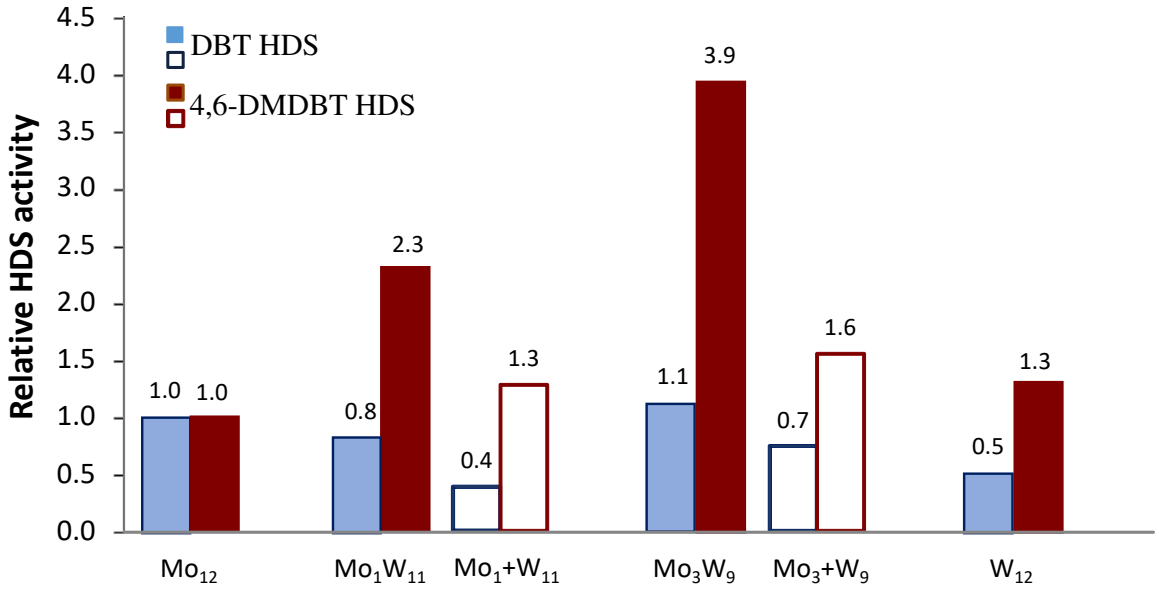

Fig. 9. Relative HDS activity of Mo(W)/Al_2O_3 catalysts in DBT and 4,6-DMDBT HDS (filled columns correspond to catalysts prepared from one precursor: Mo_{12}, W_{12}, Mo_1W_{11} and Mo_3W_9 HPA; empty columns correspond to catalysts prepared from mixtures of Mo_{12} and W_{12} HPA with 1/11 and 3/9 stoichiometry of Mo/W).

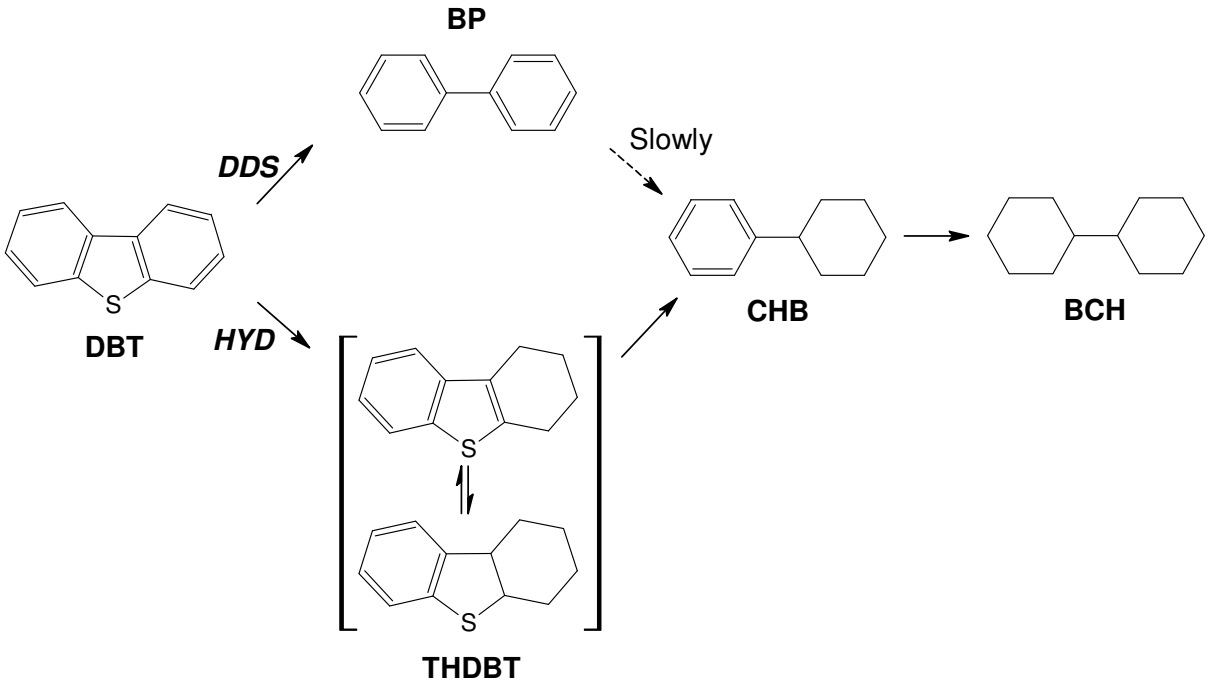

Scheme 1. Reaction network of the HDS of DBT.

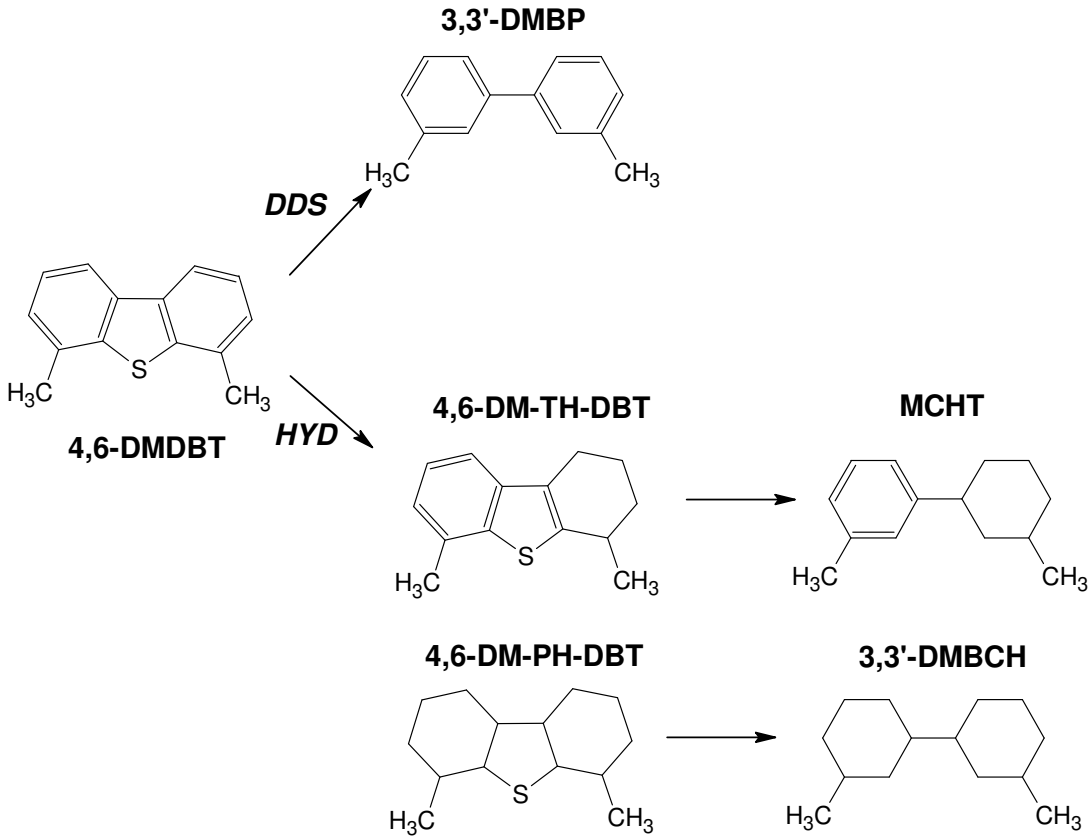

Scheme 2. Reaction network of the HDS of 4,6-DMDBT.